Refractory Residues Classification Strategy Using Emission Spectroscopy of Laser-Induced Plasmas in Tandem with a Decision Tree-Based Algorithm

Javier Moros*, Luisa María Cabalín and J. Javier Laserna

Universidad de Málaga, UMALASERLAB, Jiménez Fraud 4, ES 29010, Málaga, Spain

ABSTRACT

The recycling of refractory scraps began to be forged just over a decade ago. Until then, virtually all refractory scraps were disposed off in landfill sites without any application. Over these past few years, a growing interest and a gain steady momentum of the circular economy, the emergent framing around waste and resource management that promotes the notions of their productive cycling, has been the driving force towards the "zero waste" culture across the spectrum of refractory users and producers. In this way, the circular economy, operated following strategies such as, but not limited to, reusing, recycling, and remanufacturing, has played the pillar role in the different essential value chains of the refractory industry to the entering the new era of secondary raw material supply. In any case, prior to starting any sustainable process, it is really necessary to know the wastes and to classify them. In this context, the present research focused on a refractory residue-classification strategy based on combined laser-induced breakdown spectroscopy (LIBS) and a decision tree algorithm for a qualitative analytical performance. This tandem approach allowed the categorization of a rich set of residues in up to 10 different refractory groups. By choosing original LIBS emission intensities and intensity ratios involving the most relevant constituent elements (Al, Mg, C –through its related-species CN–, Si and Zr) of various refractory wastes, a decision tree with multiple nodes that decided how to classify inputs was designed and trained. Categorization performed from LIBS emission spectra of "*blind*" refractory residues showed that LIBS data combined with this supervised machine learning algorithm provided good refractory scraps-classification performance, with a classification accuracy of up to 75%. However, some more than justified decisions of the algorithm on allegedly misclassified residues showed that scores for the decision tree could found to be far superior to those obtained. The results achieved support the strategy designed for its industrial implementation, either directly in the iron and steel industry, as the major end-user of refractories, in the refractory waste management industry, or in both.

Keywords: laser, emission spectroscopy, decision tree, classification, refractory residues

*Corresponding author. Tel.: (+34) 951 953 015.
E-mail address: j.moros@uma.es (J. Moros)
Jiménez Fraud, 4th, Universidad de Málaga
Campus de Teatinos, 29010 Málaga, Spain

1. Introduction

Our day to day without refractories would be unimaginable. Refractory products are vital and basic elements immensely utilized in multitude of end-use industries such as iron and steel, cement, nonferrous metal, glass, ceramics, petrochemical, electric power, military, etc … to ensure the operation and production of all high-temperature industrial processes. Particularly, refractory products are one of the permanently necessary, but at the same time costliest, consumable items to steel production. The world average consumption of refractories amounts at around 10 kg per ton of crude steel. The refractory materials market size for the steel industry has the potential to grow by 5.20 million tons during 2020-2024, and the market's growth momentum will accelerate during the forecast period. Strong growth in emerging markets is the main driving force for the refractories market. Notwithstanding this, environmental concerns prove to be the major restraint for it. The declining of natural sources of raw materials and its consequent economic repercussions, an increase in the price of refractory raw materials not applicable to refractory products sold, have forced the development of a culture of harnessing based on the use of recycled spent refractory products. Making spent refractories re-usable has a positive impact in two aspects: first, the environmental part by protecting and securing the natural raw material resources in the long term and reducing energy consumption as well as lowering greenhouse gas (CO_2) emissions; and second, the economical part by stabilizing or even reducing the total cost of raw materials in manufacturing new refractories and making the production of refractories more competitive.

The use and reuse of spent refractories (secondary raw materials) either for its original purpose or for a similar purpose, or for restoring durable used refractory products to as-new condition or for recycling refractory products at the end of their useful life to create new ones for a different application are a series of actions that have as a starting point the previous characterization and classification of the material into different classes [1–3].

In this respect, there is a range of wet chemistry and dry chemistry methods for effective control of the chemical composition of refractory materials. The former, which involve techniques such as flame atomic absorption spectrometry (FAAS) –single element determination– [4] and inductively coupled plasma emission spectrometry (ICP-AES) –multi element determination– [5] may not be too advantageous due to the need to treat the samples beforehand. Instead, the less time consumed per test of dry chemistry methods [6], based mainly on radioactive –Prompt gamma neutron activation analysis (PGNAA) and pulsed fast thermal neutron activation (PFTNA)– [7], X-ray [8, 9], and laser-bearing [10] technologies. These analytical techniques can be implemented as extremely compact, non-contact, non-destructive, fast-response scanning systems designed to online measure the elemental composition on conveyor belt bulk materials.

Although neutron activation analysis is a highly sensitive method of elemental analysis it works with a radioactive source and safety measures and permits are required. In addition, surface measurement techniques such as X-ray-based ones have difficulties to cope with the fact that the surface layer may not be representative for the bulk composition. Furthermore, the X-ray is a low sensitivity approach for light elements such as Al and Mg, both distinctive elements of refractory materials. This implies long measurement times (in the order of minutes) to obtain reliable results; an impractical action in the industrial field. Thus, looking at the limitations of these technologies, laser-based systems seem to be the best candidates to undertake this kind of analysis.

Among all the laser-based technologies, LIBS (laser-induced breakdown spectroscopy) is a cutting-edge technique having several advantages over conventional elemental analysis methods. LIBS has capacity for rapidly and simultaneously detecting almost all elements after the ablation of barely a few nanograms of a target analyzed. Unlike the radiation from radioactive sources, laser radiation can at anytime be "turned off" by merely disconnecting the pumping of flash lamps. Finally, irradiation by high-repetition-rate pulse trains allows it sampling many very small areas (also in depth) on the surface of the conveyor belt [11].

From this operational aspect, LIBS has proved its capability to the on-line characterization of steel grades sequentially casted during its manufacture from the spectral information gathered during the analysis of the hot steel surface in a harsh environment as the steel plant itself [12-14].

Although, from the analytical point of view, LIBS has been used for the characterization, discrimination and classification of a wide variety of samples; from biological material [15-18], through polymeric material [19-21], pigments [22, 23], food [24, 25], and even geological samples [26-30].

Of course, to do this, LIBS has had to be used in combination with multiple chemometric strategies including approaches based on discriminant function analysis (DFA), principal component analysis (PCA) [31], partial least squares discriminant analysis (PLS-DA) [32], graph theory (GT) [33], and artificial neural networks (ANNs) [34,35], among some of them [36].

With all this, there is only one precedent for the analysis of refractory residues using LIBS, the European FP7 project REFRASORT (Innovative Separation Technologies for High Grade Recycling of Refractory Waste Using Non-Destructive Technologies, GA 603809) [37]. This project developed a LIBS system that aimed to distinguish between the three main classes of refractories used in the steel industry: class A material which is based on MgO, class B containing both MgO and CaO, and class C which is produced from mainly Al_2O_3 and SiO_2) [38].

In the present work we have gone a bit further and developed, within the framework of the project 5REFRACT (Systematic and Integral Valorization Of Refractories Under the "5r" Approach, LIFE17 ENV/ES/000228) [39], a LIBS-based classification scheme that enables a more refined identification of refractory waste. The 5REFRACT project aims at applying a 5Rs (reduce, reuse, remanufacture, recycle, re-educate) approach for the circular management of after-service refractory products within the steel sector, therefore reaching their integral valorization. The more classes into refractory wastes from the steel production activities can be identified the better the turning these industrial residues into resources.

This research proposes a classification model focusing on the categorization of used refractory samples. The analytical procedure was developed by combining emission spectral data obtained by LIBS and a non-parametric supervised learning algorithm; a decision tree.

2. Experimental

2.1. LIBS setup

A portable LIBS system designed in the UMALASERLAB, and suitable for any future use in industrial harsh environment, has been considered for the present research. Since this experimental setup has been earlier described elsewhere [40] only some details are provided as supplementary information. The most critical part of this portable LIBS system is the hand-held probe. For interested readers, **Figure S1 in Supplementary data** shows the schematic design of the compact hand-held probe containing the laser source and the optical arrangement for laser beam focusing and plasma light collection of the LIBS prototype. A Q-switched Nd:YAG pulsed laser (Ultra CFR Model, Big Sky Laser) operating at 1064 nm and generating 50 mJ pulses 6.5 ns in length is used as excitation source. A BK7 lens, of 75.6 mm in focal length and 1064 nm anti-reflexive coating, allows focusing the laser beam onto the surface of the sample. With this configuration, the spot size the diameter of the laser spot ranges around 200 µm (focused area of 0.13 mm^2). Light emitted from laser-produced plasmas is collected using a collimating lens securely attached to the tip of a 600 µm optical fiber (tri-furcated cable, 3×600 µm fibers, all legs SMA terminated, total 2 m long, splitting point in the middle) which guided the light to the entrance of a multi-channel miniature Czerny–Turner spectrograph (75 mm focal length). With this system, an effective spectral window spanning from 210 nm to 800 nm was available. Spectrometers were each one fitted with CCD detectors. Time-resolved and time-integrated measurements were synchronized to the shooting of the laser pulse. The delay time used in LIBS response acquisition was 1.28 µs, whereas the integration time was set at 1.1 ms.

The complete optical train composing the probe is located inside a prototyped housing to prevent any misalignment, damage and deterioration. Housing is equipped with a lateral entry window to achieve direct access to collimating lens for plasma light collection improvement if necessary. It has also a pre-installation

for a circuit of a buffer gas, either air to prevent ejected matter entering the housing or inert gases to perform evaluations under controlled atmosphere.

2.2. Samples

Table 1 reports the chemical composition, as oxides (% w/w), of refractory materials supplied by SIDENOR ACEROS ESPECIALES S.L. considered for the design of the initial classification model. A total of 20 refractories for continuous casting tundish, from the new unused refractories (from sample R#01 to sample R#10) and their spent (*post-mortem*) homologous materials (from sample R#11 to sample R#20), that have undergone steelmaking process, were evaluated at first.

As inferred from data in **Table 1**, refractories under consideration were mainly based on four oxides: Al_2O_3, MgO, SiO_2 and ZrO_2. Thus, according to the main chemical components, some groups could be distinguished. The first consisted of some alumina refractories (samples R#01, R#02, R#03, R#11, R#12 and R#13) having mainly acidic materials like alumina (Al_2O_3) and silica (SiO_2) with a minimum of 40 % Al_2O_3. A second group composed of magnesia-carbon refractories (samples R#04, R#05, R#06, R#07, R#14, R#15, R#16, R#17), containing fused, dead-burned (sintered) and/or large crystal sintered magnesia and 10% residual carbon (graphite). Additionally, further special products (isostatic materials for the steel industry) like alumina-magnesia-spinel brick (samples R#08 and R#18) for steel ladle lining and corundum (samples R#09 and R#19) and zircon (samples R#10 and R#20) materials used in applications such as ladle nozzles were also included.

Then, a total of 45 unknown materials were considered in a blind testing process to assess the performance of that initial classification model. Once the identity of those blind samples was known, all of them together with another set of 30 labeled wastes were used to update and improve the classification algorithm. Finally, the performance of the updated classification algorithm was evaluated with a new set of 12 blind samples.

In case it might be of interest to the reader, **Table S1**, **Table S2** and **Table S3** in **Supplementary data** report on the theoretical chemical content (expressed in % w/w of the constituent oxides) for the refractory scraps constituting the different batches used in each of these 3 last stages –evaluation, updating/improvement, performance corroboration– of the research.

2.3. LIBS sampling strategy

The refractory materials domain is highly heterogeneous. Therefore, a single LIBS spectrum cannot adequately represent it. To do a successful laser-based classification process it is necessary to have a "sampling plan", that is, clearly decide how many points must be laser-interrogated to obtain statistically significant LIBS information. While there are mathematical formulas to determine how much sampling points are needed, depending on the variation in composition, size, morphology and distribution of the particles that constitute the material, the parameters needed to use these equations are not often available when those samples are considered. Thus, to LIBS data characterize the refractory material we were trying to classify, sampling proceeded over 10 random spots over samples surface.

Furthermore, it is not easy to define the sampling section to characterize a spent refractory material. Any alteration on the chemical composition of the material and the degree of homogeneity within because of the number and type of activities and processes that it has undergone throughout the steel manufacturing is unknown. In our case, since analysis of spent refractories might provide asymmetric information from their front (contact surface with the steel being manufactured) to their back, a judgmental sampling was decided. The prior knowledge of altered surface was used to decide the sampling section, that was, the surface that had not been in contact with the steel. This action does not imply at all a bias into the analysis, because it still corresponds to a used material and is the surface that best reflects the true identity and composition of the material. In addition, a mechanical scraping of that non-exposed surface to remove grouting material that could have adhered to the side of the refractory was conducted. Any quantification to the thickness of the

layer to be removed was not attempted. Side of refractory waste was scraped using a mini electric angle grinder (3", 75mm, 280 W, from KATSU) till a surface as similar as possible to the appearance of its unused analogue was observed. Once surface ready, the aforementioned LIBS strategy for sampling was considered.

3. Results and discussion

3.1. LIBS responses of refractory materials

Alumina-based refractories

Figure 1 shows representative single-shot spectrum (the most reproducible one within the spectral series) of chamotte-based (R#01) –also grog or firesand–, andalusite-based (R#02) –an aluminum nesosilicate mineral with the chemical formula Al_2SiO_5–, and bauxite-based (R#03) –a sedimentary rock that is the most important ore of aluminum– refractories, respectively [41-43]. As inferred from data in **Table 1**, Al_2O_3 and SiO_2 are the dominant components in all them. The alumina percentage rises from 41.0 %w/w to 80.5 %w/w meanwhile that of silica declines in tandem from 54.0 %w/w to 13.0 %w/w. Thus, as seen in **Figure 1**, aluminum and silicon are well identified within the emission responses of these dense shaped refractory products of the alumina-silica series. Aluminum presence is easily identified through the doublet at 308.21 nm/309.27 nm, as well as by its most sensitive emission lines at 394.40 nm/ 396.15 nm. As far as silicon refers, the LIBS spectra show emission associated with the atomic species at 288.16 nm. Additionally, several emission lines that show the presence of elements like Ca (393.37 nm/396.85 nm and 422.67 nm, for ionic and atomic species, respectively), Na (588.99 nm/589.59 nm), Ti (498.17 nm, 499.11 nm, 499.95 nm, 500.72 nm, and 501.42 nm), Fe (302.06 nm, 404.58 nm, and 427.18 nm) and K (766.49 nm and 769.89 nm), commonly coming from minor constituent oxides, are also sometimes easily recognized. Finally, medium- and high-intensity emission signals associated to Mg (280.23 nm, 285.21 nm, 383.83 nm, 516.73 nm, 517.27 nm, and 518.36 nm), maybe from unforced impurities of the starting materials, can be also identified in those LIBS spectra.

A difference in the total emission intensity of LIBS data from these refractories was evidenced because their distinct ablation rate (amount of material removed by each laser pulse). However, a trend in the ratio of intensities for the emission signals of interest, those associate to Si and Al, was detected; a trend that fitted perfectly with the variation in stoichiometric ratio for Al_2O_3 and SiO_2 content in the samples. This circumstance seems to solve the classification of these refractories into their corresponding categories. The figure shows the most advantageous scenario. Unfortunately, the large heterogeneity within the materials derived in emission intensity ratios highly variable. This is why the categorization of these classes of materials could not be based on the ratio from a single-shot LIBS analysis. Some threshold values were needed to be defined and consolidated from the various analysis statistics.

Magnesia-based refractories

Representative single-shot LIBS spectra from laser-produced plasmas of several MgO-Carbon bricks are depicted in **Figure 2**. As inferred from data in **Table 1**, in these MgO-Carbon bricks magnesia accounted in total for around 97% in weight percentage, in form of fused or electrofused magnesite as well as sintered or dead burned magnesia. Carbon was their second major constituent, deriving in all cases from directly added flake graphite. The most relevant emission signals of Mg (reader may check wavelengths in the section before) could easily observed from LIBS spectrum. Notwithstanding this, the plasma emission spectra were well dominated by emission bands attributed to CN violet (bands heads observed at 359.0 nm, 388.3 nm and 421.6 nm) and C_2 Swan (bands heads observed at 473.7 nm, 516.5 nm, and 563.5 nm) systems. In any case, spectral lines associated to minor elements in these materials, like Si, Al, Fe and Ca, were also observed in their LIBS fingerprints.

Special attention should be given to the weak correspondence between intensity of spectral signals and mayor elements content in these MgO-Carbon bricks. As shown in the inset of **Figure 2**, virtually the same content of

Mg and C triggered different intensities ratios for the associated emission features (as can be easily deduced from the different slopes expressed as dashed lines). This is a clear sign of chemical heterogeneity, rather than a consequence of the particular ablation behavior of refractory materials under the same excitation conditions. This circumstance is corroborated by the also variable ratio of intensities for Mg and Al emissions (an element that, in theory, should not be present in the samples). The conjugation of all these facts only highlights the difficulties in cataloguing within a single class all those materials of identical chemical composition but with significantly changing LIBS fingerprints.

"Ternary-matrix" refractories

This category grouped refractory materials characterized by containing at least 3 compounds in a percentage higher than 5%, that is, more singular refractory formulations for some special applications in steelmaking, such as protection of the stream and controlling the liquid steel flow from tundish to mold. Thus, within this group were considered an alumina-magnesia-carbon (AMC) refractory brick (also spinel, R#08 and R#18), as well as a couple of refractory nozzles, mainly constituted by alumina-graphite-silica (R#09 and R#19) and zirconia-graphite-silica (R#10 and R#20), respectively. As with the graphitized magnesia-based samples (previous group), the LIBS signals of these refractory materials were dominated by the molecular emissions of CN and C_2 species; the result of their carbon content from the flaked graphite, carbon black and the phenolic resin used to all components bonded together [44–46]. Particularly, in the case of spinel (LIBS spectrum not shown), the simultaneous presence of emissions associated with Al, Mg and C is an advantage for its identification with respect to those alumina-based and magnesia-based refractories. This circumstance, a priori, is also an advantage, in order to distinguish it from the other two types of refractories that completed this group. The challenge here lied in distinguishing between the 2 types of nozzles, with the detection and identification of Zr as the main milestone. Zr is considered a more reactive metal because it traps the oxygen contained in certain refractory oxides. Therefore, it should be identified and separated so that it does not affect the processing and revalorization of the rest of the refractory residues. To expose the jigsaw puzzle, **Figure 3** depicts representative LIBS spectra of the two nozzles. As shown, the presence of alumina does not seem to be a differentiating factor, since emission signals associated with Al (the most intense ones can be seen at 308.21 nm, 309.28 nm, 394.40 nm and 396.15 nm) appeared in the LIBS spectra of samples R#10 and R#20. The fact that Al was detected in the unused sample R#10 suggested that it was due to the use of natural raw material in the manufacture of these refractory products. On the other hand, the detection and identification of Zr is much more exclusive. As observed from insets in **Figure 3**, LIBS spectrum of samples R#10 and R#20 clearly displayed the emission signals associated to the Zr: a broad spectral feature from unresolved lines at 423.93 nm and 424.17 nm and some emission signals at longer wavelengths, 468.78 nm, 471.01 nm and 473.95 nm, interspersed within the resolved fine-structure for the vibrational sequence $\Delta v=+1$ of the electronic transition ($D^3\Pi_g \rightarrow A^3\Pi_u$) of the C_2 emission spectrum. In short, it provides unequivocal proof of the existence of this component in these samples.

However, underneath this apparent simplicity of detection and identification lies the real complexity of the diagnosis. It should be noted that, the inherent heterogeneity and granulometry of the refractory materials, in fact, the particles sizes and, subsequently, the mass broad spatial distribution of these particles in contrast to the spot size of the focused laser beam, may make their point-by-point LIBS spectra qualitatively distinguishable from each other. This variability in the type and intensity of the emission lines observed may manifest not only for surface level testing but also for in-depth analysis, for which synergy between sample heterogeneity, grain-size distribution and plasma light unstability because of the crater's tunnel effect can make it a more pronounced experience.

These circumstances greatly complicate decision-making about the classification of the samples from the use of a single-shot LIBS fingerprint and the relative intensity of an identified emission line corresponding to a particular element. This is why, the across surface and in-depth LIBS scanning of the materials as well as the use of emission intensities ratios is considered the most appropriate procedure for analysis and categorization of samples. Statistics from multiple LIBS data do not correct the spectroscopic differences derived from a non-uniform chemical distribution on the sample. However, such a large data set includes many instances drawing a more representative image of what is analyzing on.

3.2. LIBS responses of refractory scraps (after-service)

Any material may have its properties or characteristics altered or modified after it has been used. Particularly, refractory materials for iron and steel production are designed to withstand the action of a harsh environment. Notwithstanding this the steelmaking process (the conditions during each use and the number of uses, if there were several) may induce a wear on the refractory working linings. These surfaces are subjected to three major types of load histories: a complex thermal history (temperature gradients and cyclic thermal loadings) that generates thermal strain and/or stress, possible phase changes, and also influence the corrosion rate; a mechanical history (dynamic loadings), especially significant when the materials are soft and weak and the structures are tall and heavy, by turbulences of the metal and slag bath that causes erosion; and chemical loadings due to non-equilibrium (difference in the chemical potential) between different mineralogical phases, which lead to chemical diffusion or reactions, therefore causing phase transformations, dissolution, and corrosion [47].

To contextualize this with a real example, **Figure 4** compares representative LIBS spectra of a chamotte-based refractory for two scenarios: when it has not been used yet and after-service. As shown, the intensities of the emission lines of the most characteristic elements differ from each to other. It is quite complex to establish a single cause for these differences. The thermal and mechanical histories may alter the ablation rate of the material, thereby modifying the amount of material removed and consequently the intensities of the emission lines for the associated elements. Furthermore, note that they are not strictly the same piece, so some differences could be due to their inherent chemical heterogeneity in addition to the chemical loadings. Variations may have a casual component, due to uncontrollable impurities in the virgin raw materials used in the manufacture of the refractories.

Particularly, in the case at hand, after-service chamotte refractory seemed to have been impoverished in elements like K (758.8°C), Na (882.8°C) and Ca (1484°C). The decrease in the content of these elements could be justified by their high volatility/low boiling temperature (see values in parentheses). However, the same was not observed for the Mg content that circumstantially seemed to increase despite its low boiling temperature (1091°C). At the same time, it seemed to have enriched in mayor elements like Al (2470°C) and Si (3265°C). However, this increase in the content of Al and Si was not attributed to any pre-concentration process but rather to a supplemented action for a deoxidation process. Al and Si are the common agents having high affinity for oxygen and added to attract it from the molten metal and form oxides, thus performing the deoxidation of the steel [48-50]. Finally, Ti content remained similar probably because of its high boiling point (3287°C).

As can be deduced from this scenario, there are numerous circumstances that can cause a whole series of non-systematic alterations on the after-service materials. All these alterations are revealed in the LIBS spectra of the material, so sorting refractory waste by using the emission lines intensities therein becomes a much more complex task.

3.3. Classification algorithm/decision tree

A decision tree-based algorithm [51] with binary splits for multiclass classification was constructed from a given set of plasma emission attributes to conduct the task of assigning refractories to one of several predefined categories. **Figure 5** illustrates the decision tree initial structure, capable of cataloguing up to 7 different classes of refractory residues. As seen, the model was an upside-down tree that made decisions according to some sorting rules based on knowledge about classified objects. The inherent chemical heterogeneity of refractory materials, together with the impurities that accompany the raw materials, in addition to the more than likely contamination after use and handling, means that the emission signals selection process was a critical step in this data analysis. Particularly in this scenario, in which the materials

shared many components albeit at different levels, classification could not rely primarily on the detection of element-specific emission lines. This is why most of the attributes considered deciding outputs were emission signal intensity ratios.

The first node within the tree-like graph picked a threshold value for the Al/Mg intensity ratio to decide between magnesia-based materials (R#04, R#05, R#06, R#07, R#14, R#15, R#16, R#17) or alumina-rich refractory products (R#01, R#02, R#03, R#08, R#09, R#10, R#11, R#12, R#13, R#18, R#19, R#20)

Then, when the abundance of Al is significantly larger than that of Mg, the classification of the refractories was complicated by a greater diversity of classes: alumina-silica systems –alumina-bearing materials catalogued as chamotte, alumina and high-alumina–, spinel –alumina-magnesia-carbon refractory–, as well as alumina-carbon and zirconia-carbon tundish nozzles. To settle these classes a set of simple nodes was sequentially applied. Thus, the first node picked a threshold value for the Al/CN intensity ratio. The value for this attribute facilitated the separation of non-carbon-containing (>15) and carbon-containing (<15) refractories. Then, the non-carbon-containing materials (R#01, R#02, R#03, R#11, R#12, R#13) were split according to a threshold value for the Al/Si intensity ratio as a predictor variable. A high Si content (synonymous with a low value for the ratio) assigned the material to the predefined category "chamotte". Meanwhile, subsequent node involving a threshold value for the Al/Ti intensity ratio as attribute distinguished category "High-alumina" (<3) from category "Alumina" (>3). In the case of assigning the carbon-containing refractories (R#08, R#09, R#10, R#18, R#19, R#20) a threshold value for the Al/Si intensity ratio was also considered as attribute: >5 will dictate category "spinel" and <5 will decide category "nozzles". Finally, the assignment to one type of nozzle or another will depend on the detection of a series of emission lines attributed to zirconium.

It is important to note that the decision tree presented here is an *ad-hoc* classification method for the categorization of refractory scraps considering the samples used for training and provided by SIDENOR, an special steel production company. However, the versatility of the strategy allowed the flowchart-like structure to be updated including new instances as well as refining the threshold values following the analysis of homologous refractory residues that have undergone different processes.

3.4. Blind-tests on after-service refractory materials

In order to check the performance of the classification method a blinded experiment was conducted. A total of 45 refractory wastes selected by SIDENOR personnel at its plant in Basauri (Bizkaia), were labeled and sent to UMALASERLAB (Málaga). **Figure S2 in Supplementary data** shows the photographs of the 45 samples to be analyzed. It should be noted that the residues examined corresponded to fragments of larger refractory pieces.

Despite the difficulties associated with different sample sizes, it was possible to establish a protocol for their analysis. A total of 6 random spots over samples surface were interrogated by 25 in-depth laser pulses each. As commented, the chemical and physical heterogeneity of the samples (the granulometry of most materials is larger than the size of the laser footprint) makes it difficult to classify them on the basis on the emission results from single-shot plasmas. However, to avoid a clash of decisions because of conflicting results derived from each of the LIBS signals, the use of the average value (n=150) of the intensity of the signals involved was considered. Results of classification accuracy after blind testing are reported in **Table 2**.

On the blind test set, 32 of 45 samples were correctly classified. Despite some errors in the assignment to specific classes, it should be noted that the algorithm perfectly distinguishes alumina-based material from magnesia-based material. Furthermore, classification errors can be discussed and argued in light of the LIBS information displayed by the materials.

Samples B#02, B#09, B#15 and B#17 were high alumina samples that the algorithm labels as alumina samples. This circumstance can be justified by the use of an element such as Ti to assign membership to one group or another. It is a minority element in both types of samples, whose optical response (emission signal at 498.17

nm) shows a significant intra-position and inter-positions large variability. To contrast the unstability of LIBS responses to this element, **Figure S3 in Supporting Information** shows graphically the emission intensities ratios for spectral signals associated to Al (at 308.21 nm) and Ti (at 498.17 nm) for the LIBS data gathered from the analysis of the 6 positions on the surface of sample B#15. Beyond the variability in the relative intensities of both emissions in the successive LIBS responses collected from the same position, there is also an unstability of this intensities ratio in the LIBS spectra from one position to another. It can be checked how for almost all positions the average value of the Al/Ti ratio was >3, therefore classifying the sample as alumina refractory. This error suggests that this input argument in the decision node is not robust enough to differentiate between these two classes of samples.

In the case of samples B#06 and B#28, they were chamotte samples mislabeled as alumina samples. This fact is justified by the similarity for the intensity ratios for the emissions associated to aluminum (at 308.21 nm) and silicon (at 288.15 nm) revealed by the LIBS information obtained in the analysis of the 6 positions on the surface of these samples to those shown by the model samples (R#02 and R#12), instead of the ratio shown by their supposedly homologous samples (R#01 and R#11). To corroborate this statement, **Figure S4 in Supplementary data** compares graphically the emission intensities ratios for spectral signals associated to Al (at 308.21 nm) and Si (at 288.15 nm) for the LIBS data gathered from the analysis of 1 from 6 positions on the surface of samples R#01 (chamotte), R#02 (alumina), B#06 and B#28. Possible explanations include the possibility of a change in the composition of the material as a result of its use or a difference in composition due to the starting material utilized for its manufacture.

Samples B#27, B#31 and B#34, although well identified as alumina-based refractories, are not correctly classified into their specific group. All they are high alumina samples that the tree labels as spinel. This circumstance is due to the detection in the LIBS response collected from the analysis of different positions of the surface of all these samples of emission characteristics associated with carbon (more specifically the signal at 388.18 nm linked to the CN species). This is why the categorization follows the spinel/nozzle branch instead of continuing for the alumina-based refractory branch.

Something similar occurs with the samples B#38, B#41 and B#43. The LIBS information collected from the analysis of some of the 6 positions on the surface of these samples, alerted to the presence of Zr. For this reason, these nozzles without Zr were catalogued as nozzles with Zr.

Because detection of carbon and zirconium in the respective samples was random, and manufacturer's statement indicated that they are products non-containing these components, only an unintentional contamination could explain these results.

Thus, while the score of ≈70% in the tree can be considered a very high value on considering the complexity and diversity of the problem, the deviation of those 13 out of the 45 samples from the expected classes, although argued, strongly affected its success rate. It is necessary to take into account that it was tried to categorizing used refractory material from a relatively small set of samples. Being congruent, only 10 samples cannot reflect the full future scenario that we may encounter. Therefore, to draw a more complete map of the variety of refractory waste and try to improve the classification success rate, we proceeded to recondition the decision tree with those 45 samples and a new set of 30 refractory residues.

Figure 6 shows the updated decision tree structure. Some changes made can be highlighted, such as a more detailed separation of magnesia-based refractories. In the event that the sample was categorized as a magnesia-based material, a first node was established to simply decide outputs between MgO-C refractories, essentially containing graphite, or other magnesia-based materials, MgO masses, by detecting the presence of CN emission signal at 388.18 nm in the LIBS spectra. Then, MgO masses can be classified according their origin into from "bloom" and from "billet", on the basis of the contents of SiO_2 and CaO. While “bloom” masses are rich in Si, the “billet” masses are characterized by a high Ca content. As far as alumina-based refractories are concerned, the first noteworthy change corresponds to the threshold value for the Al/CN intensity ratio. The updated value for this attribute assists the separation of high carbon-containing (>15%) refractories from those low- (<10%) and non-carbon-containing materials. This improves the subsequent cataloguing of some high alumina samples (sliding plate and external nozzle LF), containing carbon (7.7% and 2.7%, respectively)

and zirconium (8.5% and 5.3%, respectively). Another significant change has been the criterion for separating the spinel class from the rest of the alumina-based materials. Instead of the intensity of Si emission signal, the intensity of the Mg-related spectral feature at 280.23 nm has been considered. Finally, the analysis of a larger number of samples made it possible to adjust threshold values for the ratio of Al and Si intensities to classify the refractory waste according to its alumina content, Al_2O_3<50% for chamotte, 50%<Al_2O_3<75% for alumina, and >75% for high-alumina-based materials. It should also be noted that, with regard to the detection and identification of Zr, the same associated emission lines were considered. Thus, the confirmation of the presence of Zr in a refractory fragment was based on the simultaneous detection of 4 spectral characteristics at (423.93+424.17) nm, 468.78 nm, 471.01 nm and 473.95 nm. By using this updated decision tree structure, refractory waste could be categorized into a total of 10 different classes.

The accuracy and robustness of this updated decision tree was examined with blind tests on a new set of 12 refractory residues. Results of classification accuracy after blind testing are reported in **Table 3.** On this new blind test set, 9 of 12 samples were accurately labeled. Circumstantially, similar mislabeling to that mentioned above has been detected. The confusion of a chamotte (nB#11) by an alumina material again, forces a more thorough evaluation of the material to check through a quantitative analysis any possible deviation from its theoretical chemical composition. If it is confirmed that the same refractory product is altered differently depending on the raw material used for its manufacture, the sense of generalization of the modus operandi of the algorithm will be truncated. The same would happen if different consequences on the chemical composition of the material are corroborated because the conditions under which it has been used, that is, the type, time and temperature of the process, as well as its location in the various refractory facilities for steel casting. Similarly, the detection of Zr in residues (nB#03 and nB#05) that are not supposed to contain it also suggests the need for a multielemental determination of major-to-trace elements in these products to clarify the content, and therefore the possible origin, of zirconium therein. In any case, these evaluations are outside the focus of this research.

In summary, beyond those confusions, results herein demonstrate the efficacy of a combined LIBS detection system and decision tree as a strategy for the cataloguing of refractory residues.

Outcomes presented herein can be considered a systematic demonstration at industrial level addressing the separation of refractory residues; the key step to achieve the main objective: to turn wastes from nuisances to resources.

4. Conclusions

In the current manuscript, a novel machine learning algorithm has been successfully combined with the spectral responses obtained from a LIBS sensor for the systematic categorization of refractory residues in 10 different classes. Only the proper sorting of spent refractories allows to overcome the bottleneck of ensuring the quality of their future recycled and remanufactured materials from.

Despite the inherent chemical heterogeneity of the fresh refractory material, added to its potential alteration during the use phase, the machine learning algorithm has demonstrated to suitably drive the intrinsically multifactorial character of the LIBS analytical response. This fact puts even more value on the challenge of correctly classifying refractory residues.

It has been proved that the alteration of the used material can go beyond a mere contamination with dust and other adhesions. Its thermal, mechanical and chemical histories are relevant for the classification process. Thus, thinking about the implementation of the strategy on an industrial scale, it must be aware that the inclusion of a pre-cleaning stage on the moving objects before the analytical measurements it must be aware that the inclusion of a cleaning stage of the moving objects before their analytical measurements would only partially minimize the alterations. In addition, it has become clear that the evaluation of this type of samples requires statistics from multiple-shot LIBS spectra to minimize the effects of fluctuations in type and intensity emissions.

In any case, on considering all those numerous imponderables, a score of ≈70% for the success rate of the decision tree on categorization of refractory waste from metallurgical processes generated during the day-to-day running of a leading company in the production of steel can be considered a significantly high value.

Further research on the potential causes any chemical bias of materials either because a use itself or due to different raw materials involved for manufacture is in course. Responding to these biases and/or being able to find a pattern in the LIBS response to be modeled, could significantly help to increase the success rate in labeling new refractory residues.

CRediT authorship contribution statement

Javier Moros: Conceptualization, Methodology, Formal analysis, Investigation, Validation, Writing – original draft, Writing – review & editing. **Luisa María Cabalín:** Conceptualization, Methodology, Validation, Formal analysis, Investigation, Project administration, Funding acquisition, Writing – review. **Javier Laserna:** Conceptualization, Methodology, Supervision.

Declaration of competing interest

The authors declare that they have no known competing financial interests or personal relationships that could have appeared to influence the work reported in this paper.

Acknowledgments

This research has received funding from the European Union's LIFE Programme under contract number LIFE17 ENV/ES/000228 (LIFE5REFRACT) and from the European Commission's Research Fund for Coal and Steel under grant agreement no. 847249. The authors would like to thank David Maza and Aintzane Soto from Sidenor I+D for their contribution in the provision of samples, as well as in the discussion and interpretation of the results.

Appendix A. Supplementary data

Supplementary data associated with this article can be found, in the online version, at…

REFERENCES

[1] M. Lieder, A. Rashid, Towards circular economy implementation: a comprehensive review in context of manufacturing industry, J. Clean. Prod. 115 (2016) 36–51.

[2] G. Gaustad, M. Krystofik, M. Bustamante, K. Badami, Circular economy strategies for mitigating critical material supply issues, Resour. Conserv. Recy. 135 (2018) 24–33.

[3] L. Horckmans, P. Nielsen, P. Dierckx, A. Ducastel, Recycling of refractory bricks used in basic steelmaking: A review, Resour. Conserv. Recy. 140 (2019) 297–304.

[4] A. Shokrollahi, M. Gohari, Flame atomic absorption determination of zirconium in glass and refractory bricks after coprecipitation with aluminium hydroxide, J. Taibah Univ. Sci. 11 (2017) 540–547.
[5] E.A. Tormysheva, E.V. Melikhova, T.N. Ermolaeva, Analysis of refractory materials for metallurgy by the ICP-AES method, Inorg. Mater. 47 (2011) 1544–1547.
[6] R.C. Machado, D.F. Andrade, D.V. Babos, J.P. Castro, V.C. Costa, M.A. Sperança, J.A. Garcia, R.R. Gamela, E.R. Pereira-Filho, Solid sampling: advantages and challenges for chemical element determination—a critical review, J. Anal. At. Spectrom. 35 (2020) 54–77.
[7] L.K. Kaganov, N.M. Mukhamedshina, M.M. Usmanova, Neutron activation analysis of refractory compounds, J. Radioan. Nucl. Ch. 220 (1997) 213–216.
[8] H. Asakura, K. Ikegami, M. Murata, H. Wakita, Determination of components in refractories containing zirconia by x-ray fluorescence spectrometry, X-Ray Spectrom. 29 (2000) 418–425.
[9] M. Kuźnia, M. Rozmus-Górnikowska, A. Szajding, W. Jerzak, Chemical analysis of refractory materials by SEM technique, Metall. Foundry Eng. 38 (2012) 141–149.
[10] R. Falcone, P. Galinetto, B. Messiga, E. Negri, M.P. Riccardi, G. Sommariva, M. Verità, Combined SEM-EDX and μ-Raman spectroscopy for the characterization of glass/Al-rich refractory interfaces, Microchim. Acta 161 (2008) 381–386.
[11] A. Baryshnikov, Y. Groisman, N. Eliezer, M. Gaft, L. Akselrod, A. Savchenko, Laser-induced breakdown spectroscopy as a powerful tool for online quality control in the refractory industry, China's Refract. 25 (2016) 32–38.
[12] T. Delgado, J. Ruiz, L.M. Cabalín, J.J. Laserna, Distinction strategies based on discriminant function analysis for particular steel grades at elevated temperature using stand-off LIBS, J. Anal. At. Spectrom. 31 (2016) 2242–2252.
[13] J. Ruiz, T. Delgado, L.M. Cabalín, J.J. Laserna, At-line monitoring of continuous casting sequences of steel using discriminant function analysis and dual-pulse laser-induced breakdown spectroscopy, J. Anal. At. Spectrom. 32 (2017) 1119–1128.
[14] L.M. Cabalín, T. Delgado, J. Ruiz, D. Mier, J.J. Laserna, Stand-off laser-induced breakdown spectroscopy for steel-grade intermix detection in sequence casting operations. At-line monitoring of temporal evolution versus predicted mathematical model, Spectrochim. Acta B 146 (2018) 93–100.
[15] G. Vítková, K. Novotný, L. Prokeš, A. Hrdlička, J. Kaiser, J. Novotný, R. Malina, D. Prochazka, Fast identification of biominerals by means of stand-off laser-induced breakdown spectroscopy using linear discriminant analysis and artificial neural networks, Spectrochim. Acta B 73 (2012) 1–6.
[16] R.A. Multari, D.A. Cremers, M.L. Bostian, J.M. Dupre, J.E. Gustafson, Proof of Principle for a Real-Time Pathogen Isolation Media Diagnostic: The Use of Laser-Induced Breakdown Spectroscopy to Discriminate Bacterial Pathogens and Antimicrobial-Resistant Staphylococcus aureus Strains Grown on Blood Agar, J. Pathog. 2013, 898106.
[17] D. Pokrajac, A. Lazarevic, V. Kecman, A. Marcano, Y. Markushin, T. Vance, N. Reljin, S. McDaniel, N. Melikechi, Automatic Classification of Laser-Induced Breakdown Spectroscopy (LIBS) Data of Protein Biomarker Solutions, Appl. Spectrosc. 68 (2014) 1067–1075.
[18] M. Wang, L. Han, Z. Yang, X. Liu, Species discrimination of terrestrial processed animal proteins by laser-induced breakdown spectroscopy (LIBS) based on elemental characteristics, Biotechnol. Agron. Soc. Environ. 23 (2019) 137–146.
[19] V.K. Unnikrishnan, K.S. Choudhari, S.D. Kulkarni, R. Nayak, V.B. Kartha, C. Santhosh, Analytical predictive capabilities of Laser Induced Breakdown Spectroscopy (LIBS) with Principal Component Analysis (PCA) for plastic classification, RSC Advances 3 (2013) 25872–25880.
[20] K. Liu, D. Tian, H. Wang, G. Yang, Rapid classification of plastics by laser-induced breakdown spectroscopy (LIBS) coupled with partial least squares discrimination analysis based on variable importance (VI-PLS-DA), Anal. Methods 11 (2019) 1174–1179.
[21] D. Stefas, N. Gyftokostas, E. Bellou, S. Couris, Laser-Induced Breakdown Spectroscopy Assisted by Machine Learning for Plastics/Polymers Identification, Atoms 7 (2019) 79.

[22] V.A. Da Silva, M. Talhavini, I.C. Peixoto, J.J. Zacca, A.O. Maldaner, J.W.B. Braga, Non-destructive identification of different types and brands of blue pen inks in cursive handwriting by visible spectroscopy and PLS-DA for forensic analysis, Microchem. J. 116 (2014) 235–243.
[23] K. Rzecki, T. Sośnicki, M. Baran, M. Niedźwiecki, M. Król, T. Łojewski, U.R. Acharya, Ö. Yildirim, P. Pławiak, Application of computational intelligence methods for the automated identification of paper-ink samples based on LIBS, Sensors 18 (2018) 3670.
[24] Y. Lee, S.H. Nam, K.S. Ham, J. Gonzalez, D. Oropeza, D. Quarles Jr., J. Yoo, R.E. Russo, Multivariate classification of edible salts: Simultaneous Laser-Induced Breakdown Spectroscopy and Laser-Ablation Inductively Coupled Plasma Mass Spectrometry Analysis, Spectrochim. Acta B 118 (2016) 102–111.
[25] S. Moncayo, J.D. Rosales, R. Izquierdo-Hornillos, J. Anzano, J.O. Caceres, Classification of red wine based on its protected designation of origin (PDO) using Laser-induced Breakdown Spectroscopy (LIBS), Talanta 2016, 158, 185–191.
[26] J. El Haddad, M. Villot-Kadri, A. Ismaël, G. Gallou, K. Michel, D. Bruyère, V. Laperche, L. Canioni, B. Bousquet, Artificial neural network for on-site quantitative analysis of soils using laser induced breakdown spectroscopy, Spectrochim. Acta B 79-80 (2013) 51–57.
[27] L. Sheng, T. Zhang, G. Niu, K. Wang, H. Tang, Y. Duand, H. Li, Classification of iron ores by laser-induced breakdown spectroscopy (LIBS) combined with random forest (RF), J. Anal. At. Spectrom. 2015, 30, 453–458.
[28] Y. Zhang, Y. Li, W. Li, Z. Sun, Y. Bi, Classification of Geological Samples Based on Soft Independent Modeling of Class Analogy Using Laser-Induced Breakdown Spectroscopy, J. Spectrosc. (2018) 3683089.
[29] S. Chatterjee, M. Singh, B.P. Biswal, U.K. Sinha, S. Patbhaje, A. Sarkar, Application of laser-induced breakdown spectroscopy (LIBS) coupled with PCA for rapid classification of soil samples in geothermal areas, Anal. Bioanal. Chem. 2019, 411, 2855–2866.
[30] D. Diaz, A. Molina, D.W. Hahn, Laser-Induced Breakdown Spectroscopy and Principal Component Analysis for the Classification of Spectra from Gold-Bearing Ores, Appl. Spectrosc. 74 (2020) 42–54.
[31] L. Pagnin, L. Brunnbauer, R. Wiesinger, A. Limbeck, M. Schreiner, Multivariate analysis and laser-induced breakdown spectroscopy (LIBS): a new approach for the spatially resolved classification of modern art materials, Anal. Bioanal. Chem. 412 (2020) 3187–3198.
[32] A.M. Ollila, J. Lasue, H.E. Newsom, R.A. Multari, R.C. Wiens, S.M. Clegg, Comparison of two partial least squares-discriminant analysis algorithms for identifying geological samples with the ChemCam laser-induced breakdown spectroscopy instrument, Appl. Opt. 51 (2012) B130–B142.
[33] E. Grifoni, S. Legnaioli, G. Lorenzetti, S. Pagnotta, V. Palleschi, Application of Graph Theory to unsupervised classification of materials by Laser-Induced Breakdown Spectroscopy, Spectrochim. Acta B 118 (2016) 40–44.
[34] X. Cui, Q. Wang, Y. Zhao, X. Qiao, G. Teng, Laser-induced breakdown spectroscopy (LIBS) for classification of wood species integrated with artificial neural network (ANN), Appl. Phys. B 125 (2019) 56.
[35] J. Chen, J. Pisonero, S. Chen, X. Wang, Q. Fan, Y. Duan, Convolutional neural network as a novel classification approach for laser-induced breakdown spectroscopy applications in lithological recognition, Spectrochim. Acta B 166 (2020) 105801.
[36] T. Zhang, H. Tang, H. Li, Chemometrics in laser-induced breakdown spectroscopy: Progress of Chemometrics in Laser-induced Breakdown Spectroscopy, J. Chemom. 2018, 32, e2983.
[37] www.refrasort.eu
[38] R. Noll, C. Fricke-Begemann, S. Connemann, C. Meinhardt, V. Sturm, LIBS analyses for industrial applications – an overview of developments from 2014 to 2018, J. Anal. At. Spectrom. 33 (2018) 945–956.
[39] https://www.life5refract.eu/en/
[40] F.J. Fortes, J. Cuñat, L.M. Cabalín, J.J. Laserna, In Situ Analytical Assessment and Chemical Imaging of Historical Buildings Using a Man-Portable Laser System, Appl. Spectrosc. 61 (2007) 558–564.
[41] C.N. Djangang, A. Elimbi, U.C. Melo, G. Lecomte-Nana, C. Nkoumbou, J. Soro, J.P. Bonnet, P. Blanchart, D. Njopwouo, Sintering of Clay–Chamote Ceramic Composites for Refractory Bricks, Ceram. Int. 34 (2008) 1207–1213.

[42] J.F. Shackelford, R.H. Doremus, Ceramic and Glass Materials: Structure, Properties and Processing, Springer, Berlin, 2008.
[43] C. Sadik, I-E. El Amrani, A. Albizane, Recent advances in silica-alumina refractory: A review, J. Asian Ceram. Soc. 2 (2014) 83–96.
[44] M. Klewski, O. Lucyna, S. Michał, ArcelorMittal Refractories, Alumina-Magnesia-Carbon Bricks for Steel Ladle, in: D.G. Goski, J.D. Smith (Eds.), Proceedings of the Unified International Technical Conference on Refractories. UNITECR 2013. The American Ceramic Society, Westerville, Ohio, 2014, Ch. 123.
[45] V. Muñoz, P. Pena, A.G. Tomba Martínez, Physical, chemical and thermal characterization of alumina–magnesia–carbon refractories, Ceram. Int. 40 (2014) 9133–9149.
[46] W.A. Calvo, P. Ortega, M.J. Velasco, V. Muñoz, P. Pena, A.G. Tomba-Martinez, Characterization of alumina-magnesia-carbon refractory bricks containing aluminium and silicon, Ceram. Int. 44 (2018) 8842–8855.
[47] A. Malfliet, S. Lotfian, L. Scheunis, V. Petkov, L. Pandelaers, P.T. Jones, B. Blanpain, Degradation mechanisms and use of refractory linings in copper production processes: A critical review, J. Eur. Ceram. Soc. 34 (2014) 849–876.
[48] R. Khanna, M. Ikram-Ul Haq, Y. Wang, S. Seetharaman, V. Sahajwalla, Chemical Interactions of Alumina–Carbon Refractories with Molten Steel at 1823 K (1550 °C): Implications for Refractory Degradation and Steel Quality, Metall. Mater. Trans. B 42 (2011) 677–684.
[49] E. Benavidez, E. Brandaleze, L. Musante, P. Galliano, Corrosion Study of MgO-C Bricks in Contact with a Steelmaking Slag, Procedia Mat. Sci. 8 (2015) 228–235.
[50] W.A. Calvo, P. Pena, A.G. Tomba Martinez, Post-mortem analysis of alumina-magnesia-carbon refractory bricks used in steelmaking ladles, Ceram. Int. 45 (2019) 185–196.
[51] P. Perner, How to Interpret Decision Trees?, in: P. Perner (Ed.), Advances in Data Mining. Applications and Theoretical Aspects, ICDM 2011. Lecture Notes in Computer Science, Springer-Verlag, Berlin, 2011,Vol. 6870. pp. 40-55.

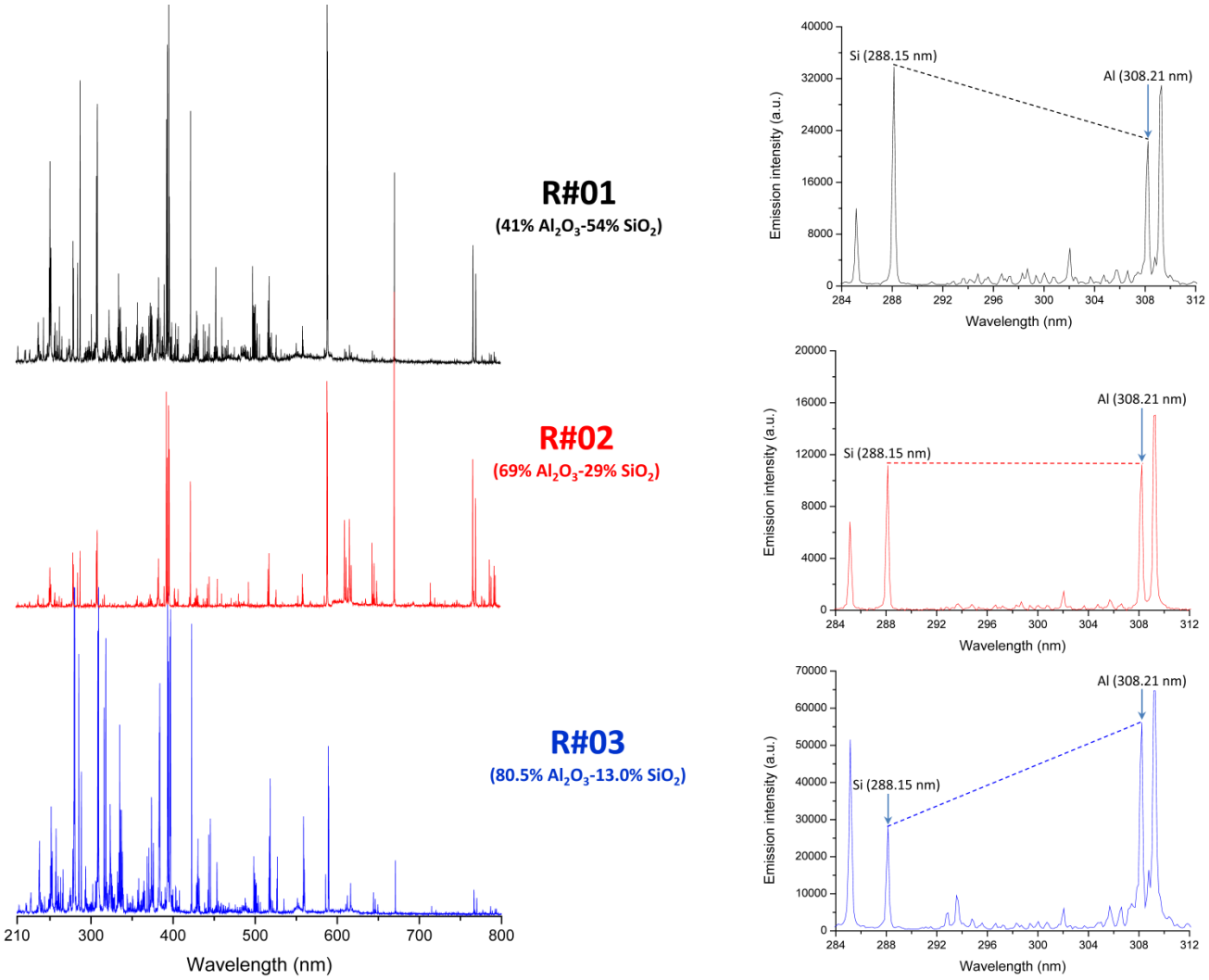

Figure 1. *Left*: Single-shot LIBS spectra in the wavelength range of 210–800 nm of refractory samples labeled as R#01 (chamotte), R#02 (alumina) and R#03 (High-alumina); *Right*: Comparison of the corresponding LIBS fingerprints in the spectral window covering from 284 nm to 312 nm with solid lines guiding, as slopes, the relationship between intensities of emissions of Al (at 308.21 nm) and Si (at 288.15 nm).

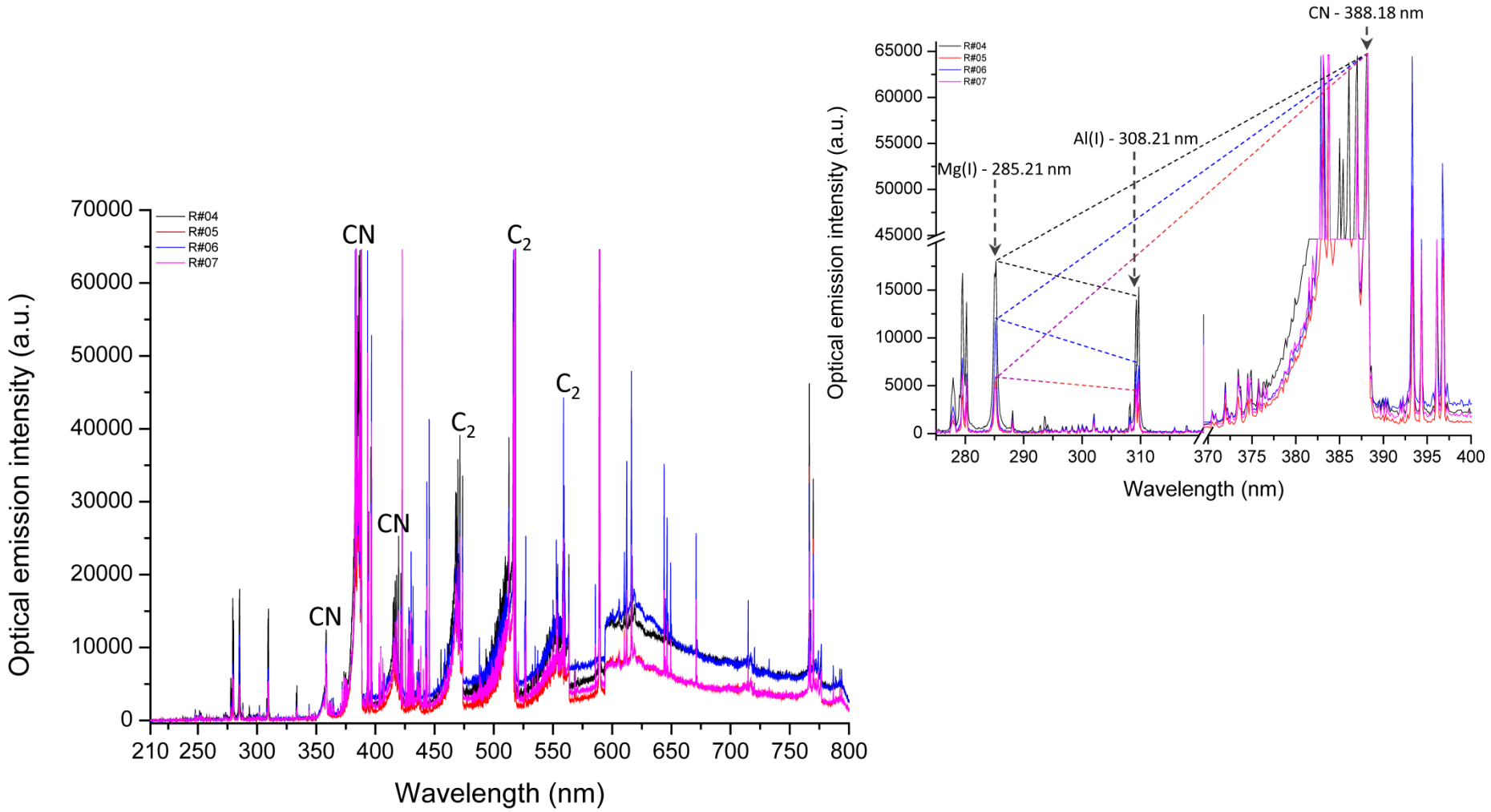

Figure 2. *Left*: Single-shot LIBS spectra in the wavelength range of 210–800 nm of MgO-C refractory samples labeled as R#04, R#05, R#06, and R#07; *Right*: Comparison of the corresponding LIBS fingerprints in the spectral windows covering from 275 nm to 320 nm and from 370 nm to 400 nm, with dashed lines guiding as slopes the relationship between intensities of emissions of Mg (at 285.21 nm) and Al (at 308.21 nm) and Mg (at 285.21 nm) and CN (at 388.28 nm), respectively.

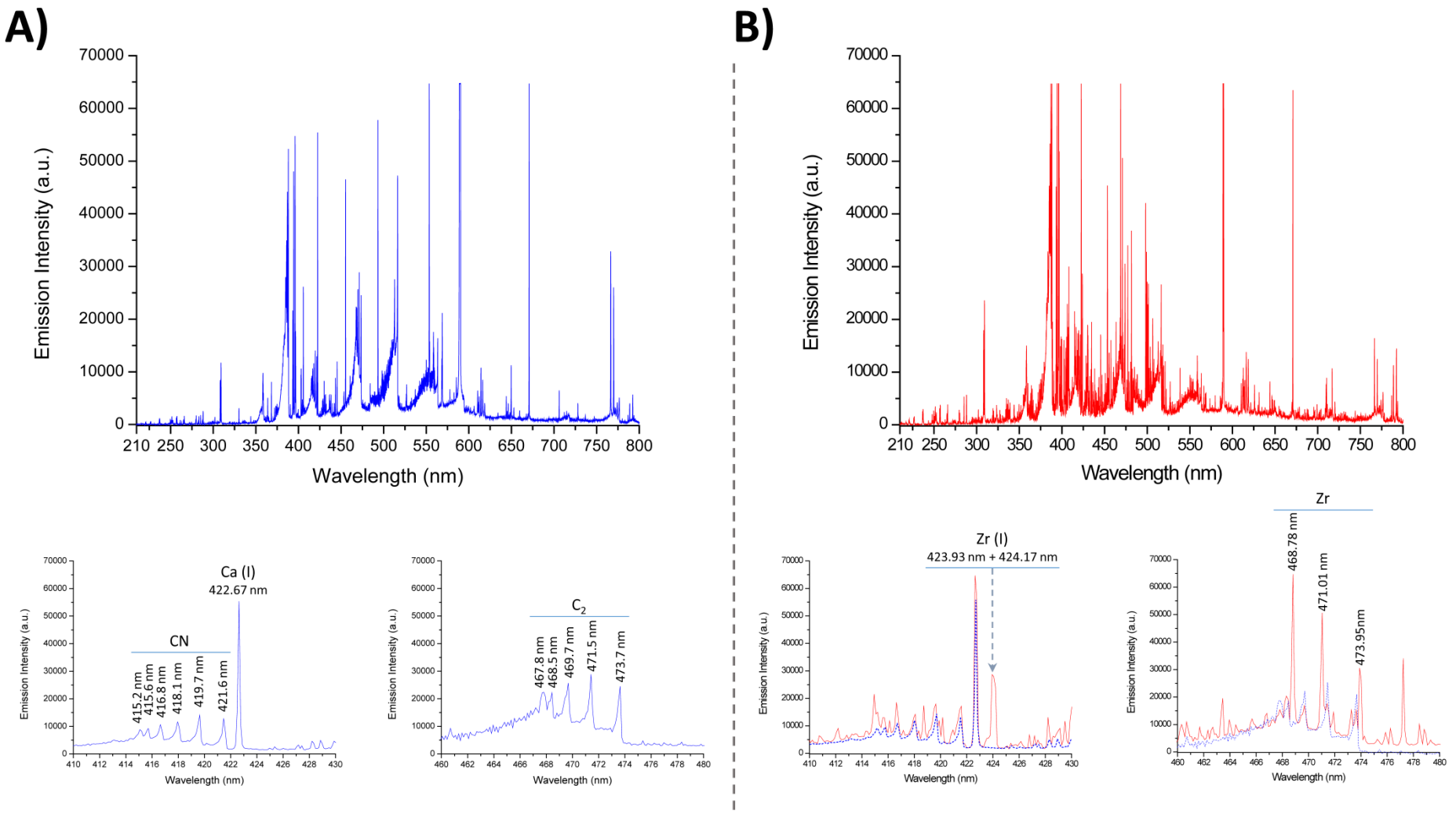

Figure 3. *Up*: Single-shot LIBS spectra in the wavelength range of 210–800 nm of refractory nozzles constituted by (A) alumina-graphite-silica (R#09) and (B) zirconia-graphite-silica (R#10); Down: Comparison of the corresponding LIBS fingerprints in the spectral windows covering from 410 nm to 430 nm and from 460 nm to 480 nm, with their most significant spectral features labeled. Note that the spectral windows of A are superimposed on B (blue dashed lines) to better evaluate the distinction of the emission lines.

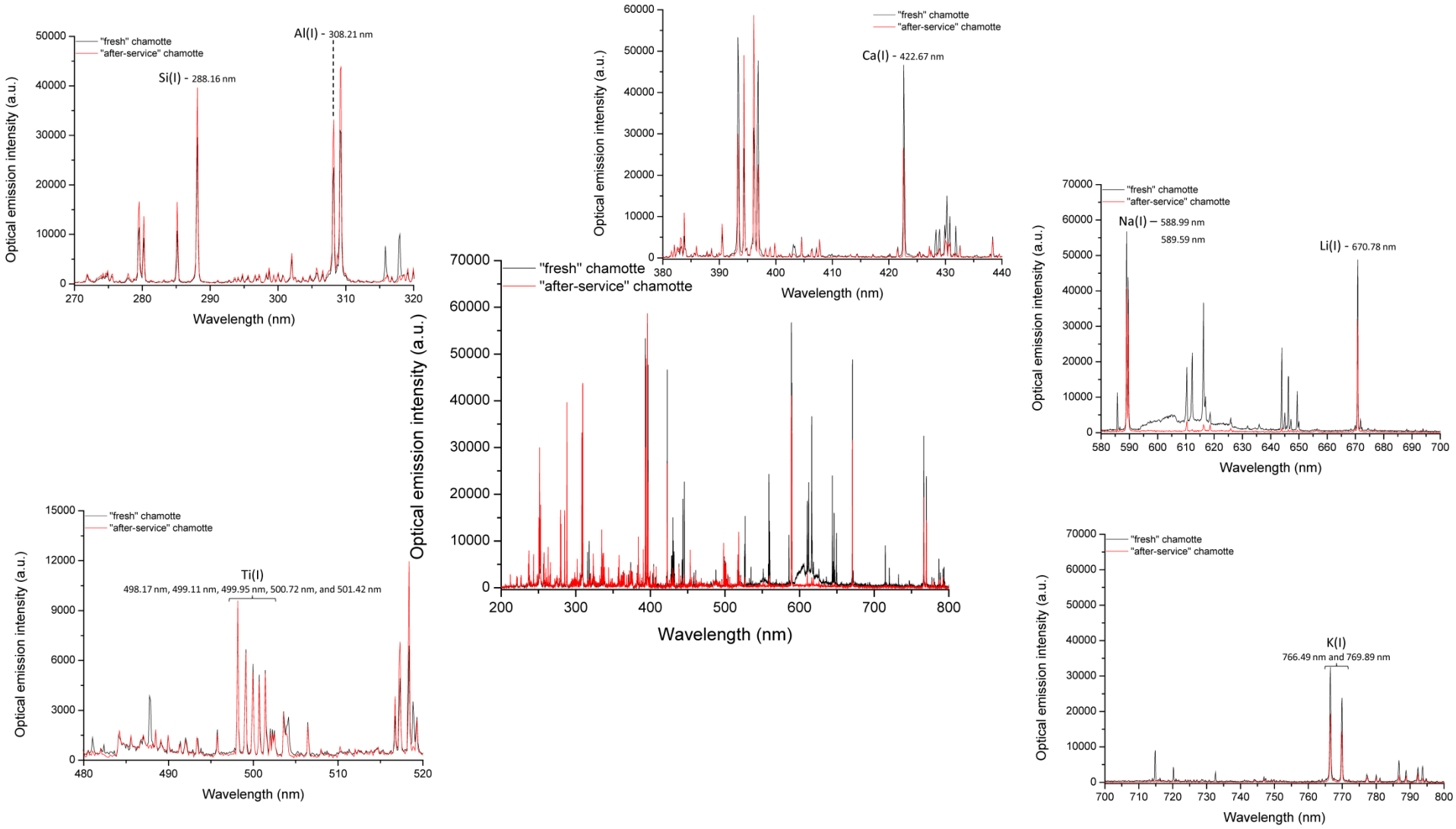

Figure 4. Comparison of the single-shot LIBS spectra in the wavelength range of 210–800 nm of "fresh" (black) and "after-service" (red) chamotte and comparison of the corresponding LIBS fingerprints in the spectral windows where the most outstanding emission lines of the constituent elements emerge. More details in the body of the text.

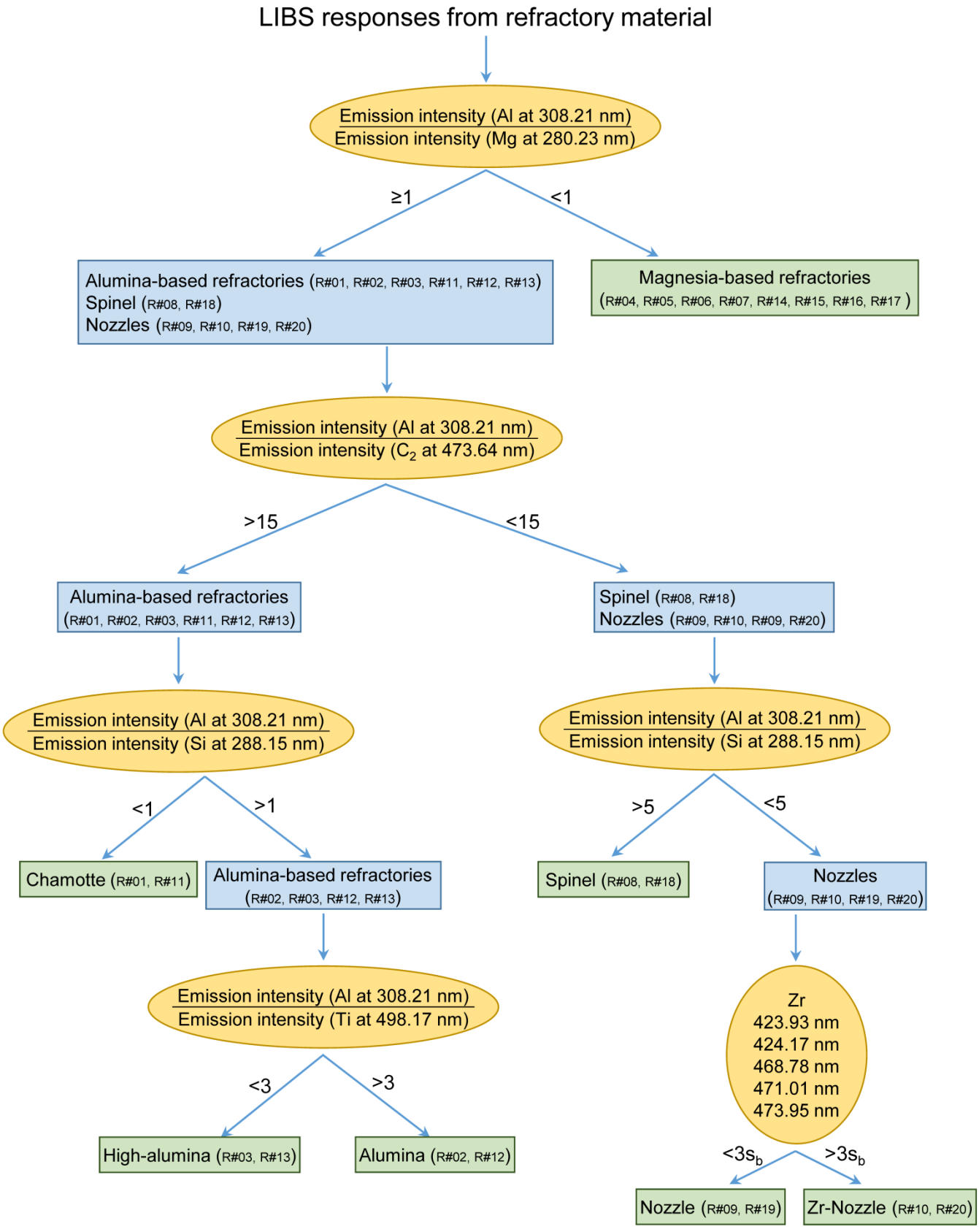

Figure 5. Structure of the initial decision tree algorithm.

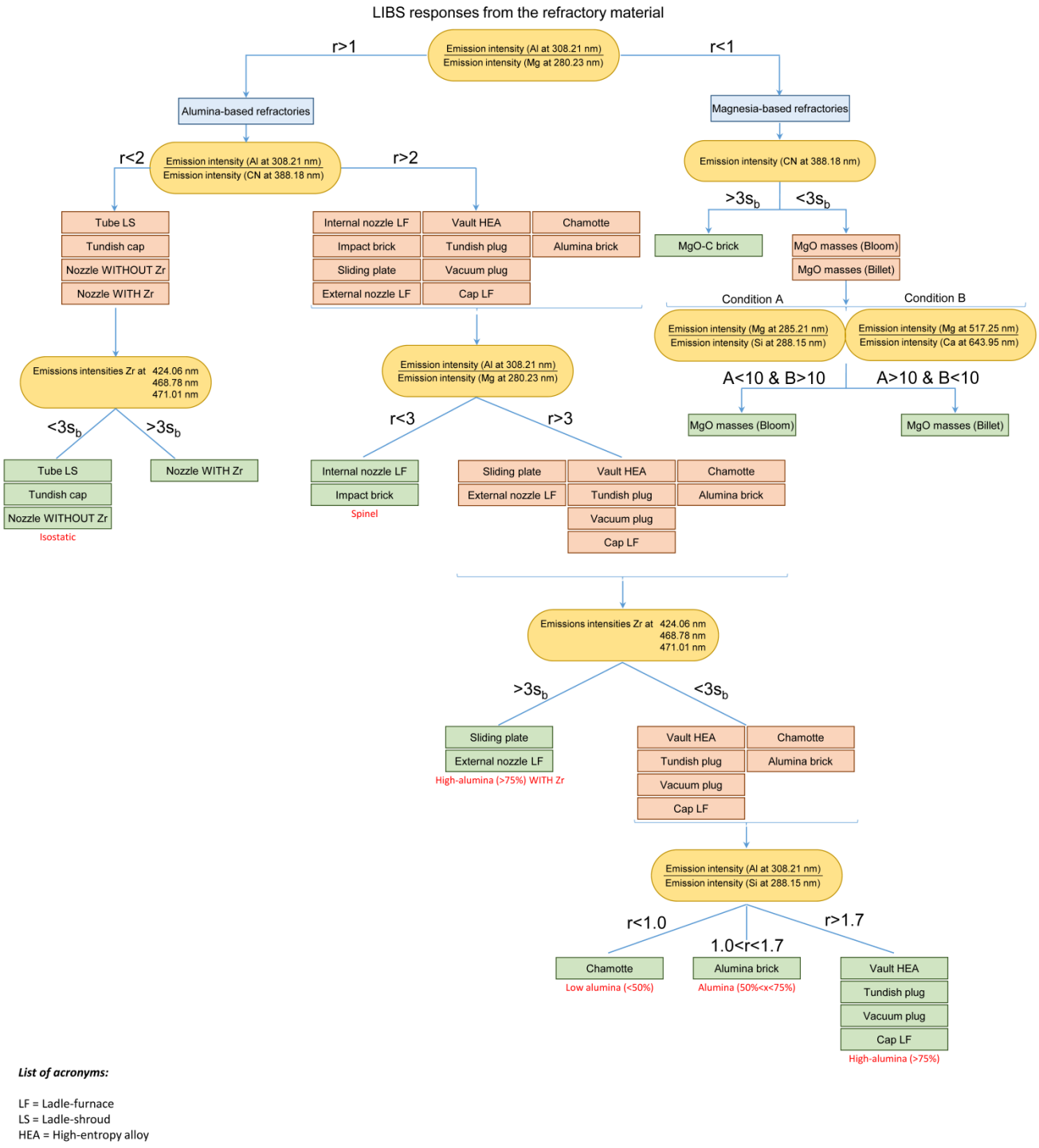

Figure 6. Structure of the update decision tree algorithm.

Table 1.- Theoretical chemical composition (% w/w of oxides) of the refractory materials considered to design the initial classification algorithm.

		Chemical composition (% w/w)									
Sample		***Al_2O_3***	***MgO***	***Fe_2O_3***	***SiO_2***	***TiO_2***	***CaO***	***K_2O***	***Na_2O***	***ZrO_2***	***C***
Unused	***Spent***										
R#01	***R#11***	41.0		1.5	54.0	1.7					
R#02	***R#12***	69.0	0.1	0.9	29.0	0.6	0.1	0.3	0.1		
R#03	***R#13***	80.5		1.4	13.0	3.1					
R#04	***R#14***	0.2	96.9	0.3	0.5		1.9				10.0
R#05	***R#15***	0.7	96.2	0.5	0.7		1.9				10.0
R#06	***R#16***	0.2	97.0	0.3	0.6		1.8				10.0
R#07	***R#17***		96.73	0.77	1.14		1.12				10.0
R#08	***R#18***	89.0	8.0	0.2	1.0	0.7	0.4				7.0
R#09	***R#19***	60.5			10.5						30.0
R#10	***R#20***				5.5					79.5	15.5

Note: Categories labelling the samples in the table can be conveniently identified from the decision tree displayed in Figure 5.

Table 2.- Summary of results of the blind test of LIBS analysis of refractory scraps. Success of assigning to membership is also presented for each residue.

Unseen Sample	*Predicted group membership*	*Actual group membership*	*Unseen Sample*	*Predicted group membership*	*Actual group membership*	*Unseen Sample*	*Predicted group membership*	*Actual group membership*
B#01	MgO-C	MgO-C	***B#16***	Nozzle without Zr	Nozzle without Zr	***B#31***	Spinel	High-alumina
B#02	Alumina	High-alumina	***B#17***	Alumina	High-alumina	***B#32***	MgO-C	MgO-C
B#03	High-alumina	High-alumina	***B#18***	High-alumina	High-alumina	***B#33***	Spinel	Spinel
B#04	MgO-C	MgO-C	***B#19***	Magnesia-based others	Magnesia-based others	***B#34***	Spinel	High-alumina
B#05	High-alumina	High-alumina	***B#20***	High-alumina	High-alumina	***B#35***	MgO-C	MgO-C
B#06	Alumina	Chamotte	***B#21***	Alumina	Alumina	***B#36***	Nozzle without Zr	High-alumina
B#07	High-alumina	High-alumina	***B#22***	Nozzle without Zr	Nozzle without Zr	***B#37***	Spinel	Spinel
B#08	Magnesia-based others	Magnesia-based others	***B#23***	Magnesia-based others	Magnesia-based others	***B#38***	Nozzle with Zr	Nozzle without Zr
B#09	Alumina	High-alumina	***B#24***	MgO-C	MgO-C	***B#39***	Magnesia-based others	Magnesia-based others
B#10	Nozzle without Zr	Nozzle without Zr	***B#25***	MgO-C	MgO-C	***B#40***	Nozzle with Zr	Nozzle with Zr
B#11	Nozzle with Zr	Nozzle with Zr	***B#26***	High-alumina	High-alumina	***B#41***	Nozzle with Zr	Nozzle without Zr
B#12	Nozzle without Zr	Nozzle without Zr	***B#27***	Spinel	High-alumina	***B#42***	Nozzle with Zr	Nozzle with Zr
B#13	Alumina	Alumina	***B#28***	Alumina	Chamotte	***B#43***	Nozzle with Zr	Nozzle without Zr
B#14	MgO-C	MgO-C	***B#29***	High-alumina	High-alumina	***B#44***	Nozzle with Zr	Nozzle with Zr
B#15	Alumina	High-alumina	***B#30***	Alumina	Alumina	***B#45***	Nozzle with Zr	Nozzle with Zr

Table 3.- Results on performance of the updated decision tree to the categorization, from LIBS data, of a new set of "blind" refractory residues.

Unseen Sample	*Predicted group membership*	*Actual group membership*
nB#01	Nozzle WITH Zr	Nozzle WITH Zr
nB#02	High-alumina	High-alumina
nB#03	Nozzle WITH Zr	Nozzle WITHOUT Zr
nB#04	High-alumina	High-alumina
nB#05	Nozzle WITH Zr	Isostatic
nB#06	MgO masses (Billet)	MgO masses (Billet)
nB#07	High-alumina	High-alumina
nB#08	High-alumina WITH Zr	Sliding plate
nB#09	Spinel	Internal nozzle LF
nB#10	High-alumina	High-alumina
nB#11	Alumina	Chamotte
nB#12	Spinel	Impact brick